

# Coated and Printed Perovskites for Photovoltaic Applications

Ian A. Howard,\* Tobias Abzieher, Ihtez M. Hossain, Helge Eggers, Fabian Schackmar, Simon Ternes, Bryce S. Richards,\* Uli Lemmer,\* and Ulrich W. Paetzold\*


Hybrid organic–inorganic metal halide perovskite semiconductors provide opportunities and challenges for the fabrication of low-cost thin-film photovoltaic devices. The opportunities are clear: the power conversion efficiency (PCE) of small-area perovskite photovoltaics has surpassed many established thin-film technologies. However, the large-scale solution-based deposition of perovskite layers introduces challenges. To form perovskite layers, precursor solutions are coated or printed and these must then be crystallized into the perovskite structure. The nucleation and crystal growth must be controlled during film formation and subsequent treatments in order to obtain high-quality, pin-hole-free films over large areas. A great deal of understanding regarding material engineering during the perovskite film formation process has been gained through spin-coating studies. Based on this, significant progress has been made on transferring material engineering strategies to processes capable of scale-up, such as blade coating, spray coating, inkjet printing, screen printing, relief printing, and gravure printing. Here, an overview is provided of the strategies that led to devices deposited by these scalable techniques with PCEs as high as 21%. Finally, the opportunities to fully close the shrinking gap to record spin-coated solar cells and to scale these efficiencies to large areas are highlighted.

## 1. Introduction

With the discovery of solution-processed hybrid organic–inorganic perovskites and the development of perovskite

Dr. I. A. Howard, I. M. Hossain, H. Eggers, F. Schackmar, S. Ternes, Prof. B. S. Richards, Prof. U. Lemmer, Dr. U. W. Paetzold  
Institute of Microstructure Technology (IMT)  
Karlsruhe Institute of Technology  
Hermann-von-Helmholtz-Platz 1  
76344 Eggenstein-Leopoldshafen, Karlsruhe, Germany  
E-mail: ian.howard@kit.edu; bryce.richards@kit.edu;  
uli.lemmer@kit.edu; ulrich.paetzold@kit.edu

Dr. I. A. Howard, T. Abzieher, H. Eggers, F. Schackmar,  
Prof. B. S. Richards, Prof. U. Lemmer, Dr. U. W. Paetzold  
Light Technology Institute (LTI)  
Karlsruhe Institute of Technology  
Engesserstrasse 13, 76131 Karlsruhe, Germany

 The ORCID identification number(s) for the author(s) of this article can be found under <https://doi.org/10.1002/adma.201806702>.

© 2019 The Authors. Published by WILEY-VCH Verlag GmbH & Co. KGaA, Weinheim. This is an open access article under the terms of the Creative Commons Attribution-NonCommercial-NoDerivs License, which permits use and distribution in any medium, provided the original work is properly cited, the use is non-commercial and no modifications or adaptations are made.

DOI: 10.1002/adma.201806702

optoelectronic devices, a novel low-cost and highly efficient photovoltaic (PV) material emerged. Only 10 years after the first reported perovskite solar cells (PSCs), power conversion efficiencies (PCEs) above 23% were certified, exceeding those of much longer established thin-film PV technologies, including organic photovoltaics (OPV) and inorganic thin-film PV based on copper indium gallium selenide (CIGS) or cadmium telluride (CdTe).<sup>[1]</sup> The material class of hybrid organic–inorganic perovskites combines excellent optoelectronic properties, such as long diffusion lengths<sup>[2]</sup> and short absorption lengths,<sup>[3]</sup> with the ease of solution processing, low energy payback times, and low-cost precursor materials.<sup>[4]</sup> Moreover, the optoelectronic properties and the material stability can be engineered by varying the constituents in the perovskite crystal structure ABX<sub>3</sub>. For example, the bandgap ( $E_G$ ) can be tuned by changing the stoichiometric ratio of Br and I at

the halogen anion site X.<sup>[5–7]</sup> In order to improve the stability of hybrid organic–inorganic perovskites, compositional engineering of the cation site A was demonstrated to be successful via combining methylammonium (CH<sub>3</sub>NH<sub>3</sub><sup>+</sup> or MA<sup>+</sup>), formamidinium (CH<sub>5</sub>N<sub>2</sub><sup>+</sup> or FA<sup>+</sup>), Cs<sup>+</sup>, and Rb<sup>+</sup> ions in the so-called multi-cation perovskites.<sup>[8–11]</sup>

Three key challenges hinder today the economical breakthrough of PSCs:

**Stability:** First, the instability of PSCs against moisture, oxygen, light, and temperature limits the lifetime of PSCs to a fraction of the warranty lifetime (often >25 years) of the market dominating crystalline silicon (c-Si) PV.<sup>[12]</sup> Very respectable progress has been made over recent years to enhance the stability of PSCs by demonstrating stability over 1000 h, but significant further advances in terms of stability are needed to lift the technology to a level where it is ready to compete with, or be a bolt-on tandem companion to the current PV heavyweight of c-Si. A number of reviews cover recent developments on the topic of stability.<sup>[13–17]</sup>

**Toxicity:** Second, highly efficient PSCs still contain lead, the toxicity of which hampers the acceptance of the technology and could conflict with legislative barriers.<sup>[18]</sup> Other recent reviews present progress with respect to this challenge.<sup>[19,20]</sup>

**Upscaling:** Third, the upscaling of perovskite PV devices to commercial PV module sizes (>1 m<sup>2</sup>) must be achieved. To date, the vast majority of research and development of PSCs is still

limited to small areas  $<1 \text{ cm}^2$ . Here, we focus on this last aspect, introducing solution-based deposition techniques that are compatible with the vision of low-cost, large-scale and high-throughput PSCs, and highlighting recent results.

Most of the scalable solution-based deposition techniques used so far to fabricate PSCs are adapted from the field of organic electronics and OPV. The most significant commercial success of organic semiconductors has come in the form of displays made from organic light emitting diodes (OLEDs). Although the current generation of this OLED technology (focusing on smaller-area displays used in smartphones) utilizes evaporation to deposit the organic materials, there is significant interest in this branch to utilize coating and printing technologies in future generations of optoelectronic products in order to reduce material wastage and enable the production of larger-area true multicolor pixel devices.<sup>[21,22]</sup> Currently, the organic materials are patterned using a shadow mask, known as a fine-metal mask (FMM), whose quality, durability, and availability over large areas currently places a major bottleneck on the next generation of device production.<sup>[21]</sup> A great deal of expertise has been generated using inkjet printing in this field, with industrial players, including Kateeva, Inc., actively contributing to its rapid further development. In the field of PV, there has also been significant effort in developing roll-to-roll PV module production,<sup>[23]</sup> commercialized, for example, by infinityPV and GCell. Based on the depth of expertise in printed electronics, it is of little surprise that there has been rapid progress in the coating and printing of perovskite materials. Herein, the unique challenges and opportunities for solution-processed PSCs are discussed, with an overview of the recent progress with regard to the most common coating and printing technologies that are of key importance to this field. This focus on printing and coating does not detract from the alternative strategy of depositing hybrid organic–inorganic perovskites by thermal coevaporation.<sup>[24]</sup> The commercial relevance of this process for large-area PV is founded in the homogeneity, high yield and ability to deposit perovskite layers on textured substrates. However, we do highlight the feasibility of reaching high-performance perovskite PV devices with industrially established coating and printing techniques, which can be integrated in large-area sheet-to-sheet as well as roll-to-roll fabrication lines.

Comparing the solution-based deposition of organic optoelectronics and perovskite optoelectronics, many similarities in the processes are apparent with regard to the ink preparation, the substrate preparation, the deposition of the solution, and the drying of the wet film (see **Figure 1**). The major differences are the nucleation step and crystallization step involved in the formation of the perovskite thin-film. For conventional solution-processed electronic materials, the ink is a solution of organic small-molecules or conjugated polymers that only undergo van der Waals bonding in the final organic thin-film; no covalent or ionic chemical bonds are formed and/or crystallization (besides the formation of limited crystalline domains in some OPV materials) takes place during the deposition.<sup>[25]</sup> Contrary to this, hybrid organic–inorganic perovskite thin films are fabricated from inks that are made of dissolved precursor materials and crystallization into the perovskite structure must occur subsequent to the wet-film deposition (see **Figure 1**). This crystallization step is of key importance for the quality and morphology of the perovskite



**Ian Howard** leads the Advanced Materials and Optical Spectroscopy group at the Karlsruhe Institute of Technology. He received his Ph.D. from the University of Cambridge under the supervision of Prof. Neil Greenham, then held a Humboldt postdoctoral fellowship at the Max Planck Institute for Polymer Research in Mainz. Since 2014 his group at the Karlsruhe Institute of Technology has focused on understanding and developing optoelectronic materials and devices, including photovoltaic cells and lasers.



**Uli Lemmer** received his Diploma degree from RWTH Aachen University in 1990 and his Ph.D. from the University of Marburg in 1995. From 1995 to 1996, he held a postdoctoral position with the University of California at Santa Barbara. He headed the Organic Optoelectronics group at the University of Munich from 1996 to 2002. In 2002, he was appointed a full professor and the director of the Light Technology Institute, Karlsruhe Institute of Technology (KIT). Since 2006, he has also been the coordinator of the Karlsruhe School of Optics & Photonics (KSOP).



**Ulrich W. Paetzold** leads the research group Advanced Optics and Materials for Next Generation Photovoltaics at Karlsruhe Institute of Technology. He was a doctoral student at Forschungszentrum Jülich and received his Ph.D. in physics from RWTH Aachen University, then continued as a postdoc at imec in Leuven. In 2016, he was awarded an independent research group at Karlsruhe Institute of Technology. His research focuses on the interaction between light and structured matter for the purpose of engineering novel optical concepts and nanophotonic materials for solar energy harvesting. He is particularly interested in perovskite thin-film photovoltaics and perovskite-based multijunction photovoltaics.

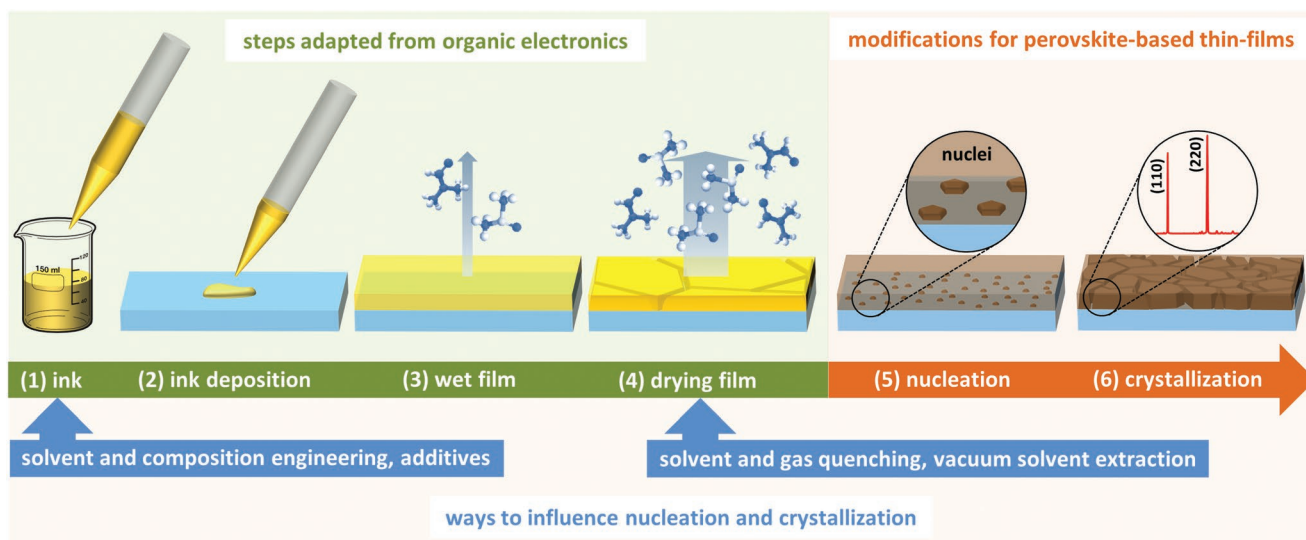


**Figure 1.** The steps involved in the solution-based deposition of perovskite thin films. Optimizing the nucleation and crystallization is critically important for the formation of high-quality perovskite absorbers.

thin-film.<sup>[26,27]</sup> In most cases, the desirable morphology of the perovskite thin-film features a large grain size, a dense film (exhibiting as few pinholes as possible), and a low surface roughness. These criteria should be met while maintaining a uniform perovskite crystal structure and phase throughout the bulk absorber.<sup>[7,28]</sup> Using the low-throughput, but laboratory-friendly, spin-coating technique, strategies to foster the formation of such high-quality perovskite thin-films have been extensively documented in literature.<sup>[29]</sup> These strategies, which also play an important role for the coating and printing techniques discussed below, include: a) solvent engineering also called ink formulation engineering,<sup>[30–36]</sup> a method that combines solvents of different boiling points to control the solvent evaporation and in turn the crystallization; b) additives<sup>[37–40]</sup> in the precursor ink to initiate the crystallization of the perovskite thin-film; c) engineering the composition of the precursor materials to impact the crystallization dynamics (through one-step and two-step deposition routes)<sup>[8,10,28,41]</sup>; d) solvent quenching,<sup>[8,42–44]</sup> by adding so-called antisolvents to the wet film that rapidly remove the ink solvent from the wet film and initiate a prompt crystallization; e) vacuum solvent extraction, similarly using vacuum extraction of the ink solvent from the wet film to prompt crystallization<sup>[32,45]</sup>; and f) gas quenching<sup>[46,47]</sup> and gas drying,<sup>[48–50]</sup> again to push out the solvent from the wet film and assist with rapid crystallization. The application of these strategies developed at the laboratory scale is possible in scalable printing and coating techniques as discussed below.

## 2. Coating and Printing Techniques for Perovskite Photovoltaics

Although spin coating continues to pioneer laboratory-scale studies to control and optimize PSC film morphology, the techniques and understanding from these laboratory-scale results must be transferred into a scalable, high-throughput coating processes to yield closed films with large perovskite

grains. As detailed below, some general approaches such as developing ink formulations that expand processing windows have the possibility to impact many coating technologies (for example, by enabling crystal nucleation by nonsolvent extraction techniques to be applied minutes after a wet film is deposited),<sup>[33]</sup> while other approaches are specific to given coating techniques. In general, significant progress has been made in the quality of perovskite films deposited rapidly over large areas in the last few years, and if progress continues at this pace there should be competing coating techniques that fulfil the technical requirements for industrial deposition of perovskite thin-films for PSC.

Before beginning the review, we make a few notes regarding the caution that must be exercised when comparing *PCEs* of PSCs, and our approach to handling comparisons. Given the hysteresis in their current–voltage (*J–V*) characteristics, the *PCE* of a PSC derived from *J–V* characteristics often deviates from the *PCE* determined by a stabilized power output measurement. For this reason, although we often present *PCEs* derived from *J–V* curves (if no further information is given a *PCE* is derived from the *J–V* curve), we also consider the stabilized efficiencies (clearly labelled as such) when comparing record devices. We also note, that although there are different methods for determining a stabilized power output efficiency; the reader interested in highly precise comparison is advised to check the experimental conditions in the original sources. Finally, when moving from solar cells to PV modules it should be noted that *PCEs* are currently not reported in a consistent way in the field. From the application point of view, the *PCE* of perovskite PV modules should be reported with respect to the aperture area (including the active area and the dead areas needed for thin-film module interconnection). In the future, it is strongly desired that module efficiencies be presented with respect to aperture area (or even total module area). However, many of the early publications in the field have reported only the *PCE* with respect to the active area. *PCEs* quoted with respect to the smaller



active area are naturally increased relative to those quoted with respect to aperture area. This allows, for example, wide interconnects optimized for excellent transport but occupying too much area for final PV module design to be used. In this sense, it is not a useful metric for the further development of perovskite modules with relevance for practical application. In order to clearly differentiate between these cases in this review, we preferentially refer to the aperture area *PCE* but occasionally mention active area *PCEs* when no alternative is possible. From an ultimate use perspective and for the further development of the field, the aperture area definition of the efficiency is relevant and must be used.

## 2.1. Blade Coating and Slot-Die Coating

Blade coating—also known as knife coating or bar coating (with a cylindrical bar with or without wire coils instead of the blade)—is a robust process with low investment cost, suitable for rigid or flexible substrates. In order to deposit a thin film, the ink is dropped in front of the blade that is then swept forward relative to the substrate. For this, either the blade or the substrate is moved to create a homogenous wet thin film (see Figure 2a). The thickness of the deposited thin-film depends mainly on: 1) the meniscus that the solution forms between blade and substrate and 2) the material concentration in the

ink. The former is controlled by the gap between blade and substrate, the speed of the blade relative to the substrate, the viscosity of the ink, the geometry of the blade, and the substrate wettability.<sup>[25]</sup>

Slot-die coating is a process particularly suitable for roll-to-roll processes as it offers continuous ink supply. The slot-die head, two independently moveable metal blades forming a slit on the bottom side, is placed with a fixed gap over the substrate. Integrated to the slot-die head is an ink reservoir, which is connected to a solution pumping system that supplies ink at a certain rate (see Figure 2b). During deposition, the solution forms an up- and a downstream-meniscus between the head lips and the substrate. In addition to the parameters discussed above for blade coating, such as the gap between the slot-die head and the substrate (see Figure 2d), the pumping rate of the solution influences slot-die coated film deposition. By attaching a mask onto the head and block partly the slit, it is possible to print striped patterns with a resolution down to several hundreds of micrometers. Moreover, the slot-die head can be held at elevated temperatures to manipulate the viscosity and the solubility of the solids in solution.

There are many reports of high-quality perovskite thin-films deposited by slot-die coating and blade coating (see Table S1, Supporting Information). Either a one-step route or a two-step route is used to deposit perovskite thin-films by blade or slot-die coating. For the two-step route, typically a  $\text{PbI}_2$  layer

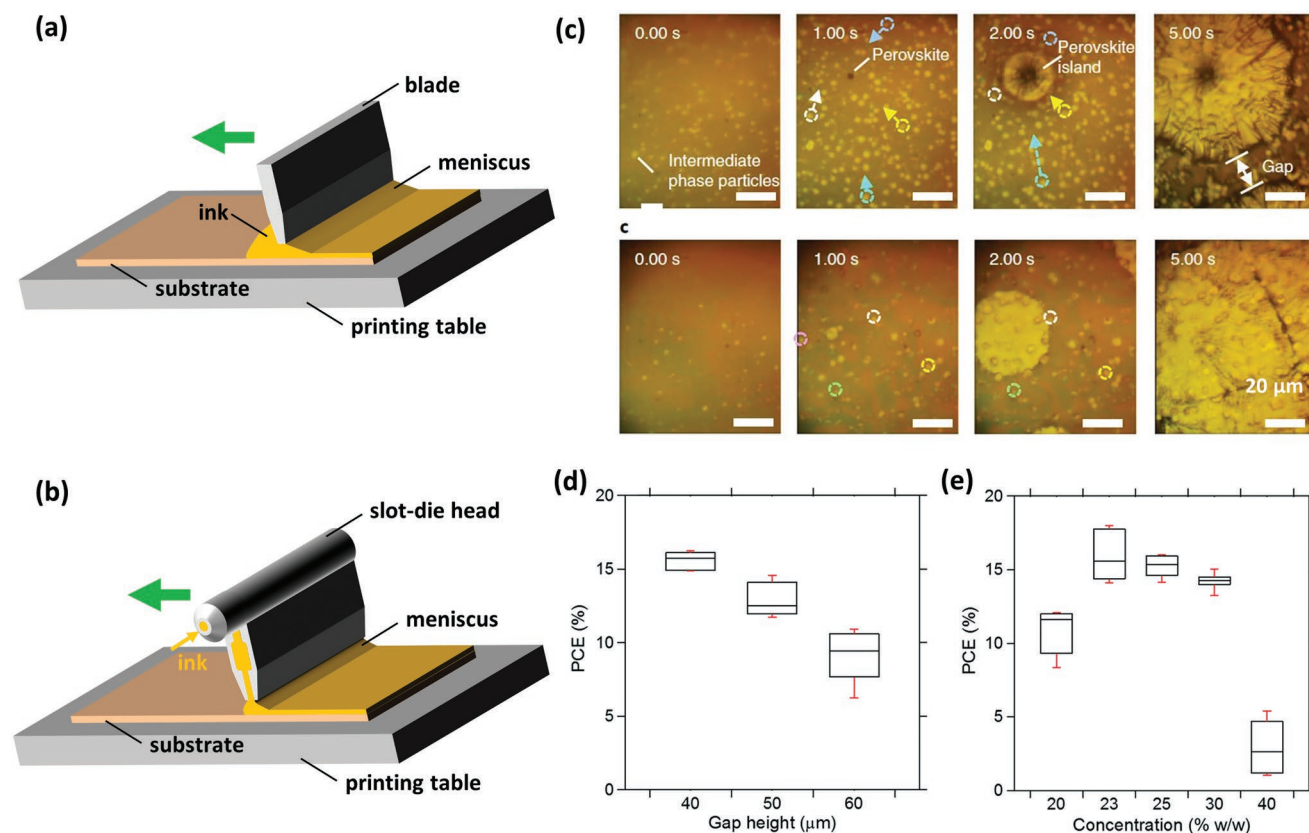


**Figure 2.** Blade coating and slot-die coating. a,b) Schematic illustration of blade coating (a) and slot-die coating (b). c) In situ microscopy observations during drying of the perovskite ink during blade coating without (top row) and with (bottom row) surfactants. c) Reproduced with permission.<sup>[64]</sup> Copyright 2018, Springer Nature. d,e) The quality of the coated perovskite layer depends on gap height (d) and ink concentration (e). d,e) Reproduced with permission.<sup>[73]</sup> Copyright 2016, Royal Society of Chemistry.

is deposited via slot-die coating first and subsequently, either an ink containing the cation and the remaining halogen is coated on top of the  $\text{PbI}_2$  layer or the substrate is simply dipped in such a solution containing the cation and the halogen, inducing the formation of perovskite. In the more common one-step route, the coated precursor solution contains already all chemical components of the perovskite crystal structure. The workhorse material in the field and also most commonly used perovskite material for slot-die and blade coating is methylammonium lead iodide ( $\text{CH}_3\text{NH}_3\text{PbI}_3$  or  $\text{MAPbI}_3$ ), which can be deposited from various combinations of the following precursors:  $\text{PbI}_2$ ,  $\text{PbCl}_2$ ,  $\text{Pb}(\text{C}_2\text{H}_3\text{O}_2)_2$ ,  $\text{MACl}$ , and  $\text{MAI}$ . Moreover, additives like  $\text{NH}_4\text{Cl}$ ,<sup>[51]</sup>  $\text{DIO}$ <sup>[52–55]</sup> (1,8-diiodooctane), or  $\text{HPA}$ <sup>[56]</sup> (hypophosphorous acid) have demonstrated to support the formation of high-quality perovskite thin-films via blade coating and slot-die coating. However, with the emergence of the more stable multi-cation perovskites in the last three years, most current research is directed toward these perovskite materials. As one of the first studies, Deng et al. investigated the blade-coated  $\text{FA}_{0.4}\text{MA}_{0.6}\text{PbI}_3$  double-cation system and compared the performance to  $\text{MAPbI}_3$ .<sup>[57]</sup> Heo et al. upscaled the slot-die deposition technique for multi-cation perovskites, depositing the multi-cation perovskite  $\text{FA}_{0.4}\text{MA}_{0.6}\text{PbI}_3$  via a roll-to-roll sequential two-step process onto foils and demonstrating flexible PSC with 11% in *PCE*.<sup>[58]</sup> Di Giacomo et al. further improved the ink formulation and drying parameters to deposit  $\text{Cs}_{0.05}\text{MA}_{0.15}\text{FA}_{0.8}\text{PbI}_{2.55}\text{Br}_{0.45}$  and  $\text{Cs}_{0.15}\text{FA}_{0.85}\text{PbI}_{2.55}\text{Br}_{0.45}$  via slot-die coating and achieved 16% stable power output efficiency.<sup>[59]</sup> Beyond this, a stable power output efficiency >19% for over 5 min was demonstrated for blade-coated multi-cation PSC by Tang et al. using elevated substrate temperatures of up to 150 °C and gas quenching.<sup>[60]</sup> For shorter stabilization times (75 s) Wu et al. demonstrated a *PCE* as high as 20% for an HTL-free device architecture employing doped  $\text{MAPbI}_3$  absorber layers.<sup>[61]</sup> Recently, Duo et al. used a highly concentrated solution in a lower boiling point solvent (methylamine-charged acetonitrile) to substitute dimethylformamide (DMF).<sup>[62]</sup> This allowed very rapid crystallization dynamics (<1 s) that led to more uniaxially oriented perovskite grains (fewer grain boundaries in the blocking transport in the vertical direction). This led to fully coated PSCs with several perovskite absorbers, i.e.,  $\text{MAPbI}_3$  (18.2% stabilized *PCE*) or wide-bandgap  $\text{FA}_{0.125}\text{MA}_{0.875}\text{PbI}_2\text{Br}$  (1.71 eV, 13.9% initial *PCE*).<sup>[62]</sup>

The drying and crystallization in blade-coated perovskite thin-films is controlled by substrate temperature, gas quenching, solvent quenching approaches, and vacuum-induced crystallization. In most cases, elevated substrate temperatures between 40 °C and 165 °C are used for blade coating.<sup>[60,61]</sup> Alternatively, for slot-die coating, dry air or  $\text{N}_2$ -streams are often employed to accelerate the solvent evaporation and for gas quenching in order to induce a rapid crystallization of the perovskite thin film.<sup>[51,63]</sup> A key advantage of gas quenching over solvent quenching, which is the most established route to induce fast crystallization in spin-coated multi-cation perovskite films, is that a gas supply and exhaust is in principle very simple to implement in a roll-to-roll process and requires no subsequent drying time. Nevertheless, solvent quenching was also very successfully employed for

slot-die and blade-coated perovskite thin-films, in particular if the rather short time window for the solvent quenching step is extended by employing high boiling point solvents in the ink. In this way, Yang et al. demonstrated PSCs with stable power output efficiency of 19% *PCE* on small-area (0.12 cm<sup>2</sup>) devices and 13.3% *PCE* for >10 cm<sup>2</sup> perovskite PV modules (12.2 cm<sup>2</sup> aperture area).<sup>[33]</sup> Another very innovative route to control crystallization of the perovskite film was presented by Deng et al., who added surfactants to suppress the fluid and particle flow during the drying of the wet film, resulting in homogeneous films (see Figure 2c) and small-area  $\text{MAPbI}_3$  PSCs (<0.75 cm<sup>2</sup>) with *PCE* of 20.3% as well as a perovskite PV module (57.2 cm<sup>2</sup>, aperture area) with stable power output efficiency of 14.6%.<sup>[64]</sup>

In addition to the deposition of the perovskite absorber layer itself, the charge transport layers can be blade- or slot-die-coated as well. This is essential for the ultimate goal of perovskite PV upscaling, the realization of all-printed/-coated device architectures. All-blade-coated devices have been demonstrated in literature with a stable power output efficiency of 18.2%.<sup>[62]</sup> In addition, several groups developed all-slot-die-coated devices,<sup>[59,65–68]</sup> the best solar cells reaching up to 16% in stable power output efficiency,<sup>[59]</sup> and a combination of the both coating techniques.<sup>[62,69]</sup> Up to date, not only hole transport layers (HTLs) like the polymers PEDOT:PSS<sup>[52,58,70,71]</sup> (poly(3,4-ethylenedioxythiophene):(polystyrene sulphonate)), P3HT<sup>[65,72]</sup> (poly(3-hexylthiophene)), and PTAA<sup>[64]</sup> or small molecules like Spiro-OMeTAD (2,2',7,7'-tetrakis(*N,N'*-di-*p*-methoxy phenylamine)-9,9'-spirobifluorene)<sup>[66,67]</sup> and Bifluoro-OMeTAD,<sup>[58,67]</sup> but also electron transport layers (ETLs) like the fullerenes  $\text{C}_{60}$ <sup>[52,56]</sup> and  $\text{PCBM}$ <sup>[52,56,69]</sup> ([6,6]-phenyl- $\text{C}_{61}$ -butyric acid methyl ester) and dispersed inorganic metal oxide nanoparticles like  $\text{NiO}_x$ ,<sup>[56]</sup>  $\text{ZnO}$ ,<sup>[58,65,67,71]</sup>  $\text{SnO}$ ,<sup>[59,62,68]</sup> or  $\text{TiO}_2$  have been successfully deposited by blade coating and slot-die coating.<sup>[66]</sup>

In summary, blade-coated PSCs demonstrated *PCE*s exceeding 20% for small-area solar cells and >14% for laboratory-scale PV modules (57 cm<sup>2</sup>, aperture area).<sup>[64]</sup> Similarly, slot-die-coated PSCs resulted in *PCE* ≈ 18% for small-area solar cells<sup>[73]</sup> and 13.8% for PV modules (144 cm<sup>2</sup>, aperture area).<sup>[74]</sup> The progress in the literature indicates that the key challenge of controlling nucleation and crystallization to obtain high-quality pinhole-free perovskite absorber layers over large can be mastered well. With regard to upscaling blade and slot-die coating for perovskites, the most attractive routes to control the perovskite crystallization appear to be substrate temperature, solvent engineering, and gas quenching, all of which can be applied in roll-to-roll processes. Gas quenching seems to be favorable over solvent quenching due to its simplicity and roll-to-roll fabrication suitability. In general, slot-die coating and blade coating are, both, well-established industrial deposition techniques processes which can operate at very high deposition rates, making them promising candidates for upscaling perovskite PV.

## 2.2. Inkjet Printing

Inkjet printing is one of the most widely used printing techniques given its commercial success in office printers. In recent years, inkjet printing has advanced toward a competitive

deposition method for inorganic and organic optoelectronics.<sup>[75–80]</sup> The key advantages of inkjet printing are that it is a material-efficient, contactless process with great flexibility in terms of the printed shape, thickness, and flexibility in the shape of the digitally printed layers. However, the key challenge for this technology is still to retain these benefits at high throughput.

The two most established inkjet printing methods are continuous inkjet printing (CIJP) and drop-on-demand (DoD) printing. The latter is more material-efficient, allows higher resolutions and has therefore proven more relevant to the industrial manufacturing of electronics to date.<sup>[81]</sup> The general principle of a DoD inkjet printer is displayed in **Figure 3a**, where the printer head is mounted over the substrate table, with at least one of them being movable. The printer head is connected to a continuous supply of ink. A pressure pulse in the fluid controls the ejection of ink from the print head. This pulse is generated by either local heating of the ink or mechanical force on the ink reservoir by a piezoelectric transducer. Since the ejection of material via heating entails an additional demand on the ink, most industrial DoD printers are piezoelectrics based.<sup>[81]</sup> A great variety of inks can be used, but ink formulations must be found that have the correct dynamic viscosity, density and surface tension to function correctly in the print head.<sup>[82,83]</sup> Also, for a given substrate surface, the ink may need to be adjusted in order to avoid unwanted surface interactions, e.g., de-wetting and nonuniform coverage or drying (such as “coffee-rings”).<sup>[84,85]</sup>

Inkjet printing of efficient OPV has been demonstrated in 2007.<sup>[86]</sup> Inkjet printing was also used to produce PSCs soon after their discovery. In 2014, Yang et al. utilized inkjet printing to fabricate HTL-free and metal-electrode-free PSC in a two-step process by inkjet printing MAI on top of a spin-coated  $\text{PbI}_2$  layer.<sup>[87]</sup> In comparison to the  $\text{PbI}_2$  layer being exposed to a MAI solution, the inkjet-printed approach with mixed ink demonstrated better crystallinity and an improved  $\text{MAPbI}_3/\text{carbon}$  interface, which ultimately led to a higher *PCE* of 11.6% (compared to 8.5%). The first one-step inkjet-deposited PSC was demonstrated in the same year. Li et al. made an ink of

$\text{PbI}_2$  and MAI dissolved in  $\gamma$ -butyrolactone (GBL) and employed inkjet printing to deposit it on top of a mesoporous  $\text{TiO}_2$  ETL. By adding MAI to the ink and heating the substrate during printing, the *PCEs* were improved to 12.3%.<sup>[88]</sup> Similar results were achieved by Mathies et al., who established a vacuum solvent extraction step to initiate a prompt crystallization, resulting in a *PCE* of 11.3% with an open-circuit voltage ( $V_{\text{OC}}$ ) of 1.0 V.<sup>[32]</sup> Bag et al. demonstrated that inkjet printing could also play a valuable role in research, by facilitating combinatorial screening of new materials.<sup>[89]</sup> These authors demonstrated in situ mixing of inks to rapidly vary the cation ratio over a number of printed solar cells by using a print head with four ink reservoirs. By printing different ratios of MAI and formamidinium iodide (FAI) on a spin-coated  $\text{PbI}_2$  layer the *PCE* was optimized to 11.1%.<sup>[89]</sup>

The stability of inkjet-printed PSCs is comparable to other solution-based deposition techniques. For example, an inkjet-printed device using  $\text{MAPbI}_3$  with a *PCE* of 9.5% remained stable for >1000 h of continuous illumination.<sup>[90]</sup> Another approach toward stability is to use multi-cation perovskite with a combination of MA-, FA- and Cs-ions at the cation site, Mathies et al. developed a suitable ink for inkjet printing and achieved a high *PCE* of 15.3% with a high  $V_{\text{OC}}$  of 1.06 V in a stack with spin-coated  $\text{TiO}_2$  and Spiro-OMeTAD as ETL and HTL, respectively. The power output maintained >90% of its initial *PCE* over >100 min of measurement.<sup>[91]</sup> A strong influence of the thickness on the perovskite absorber (affecting properties such as grain size) was observed (see **Figure 3b–d**).

The scalability and flexibility of inkjet printing as deposition method for PSCs has also been explored.<sup>[92,93]</sup> In 2018, first perovskite PV modules with an area of >2  $\text{cm}^2$  were reported. For example, by using a  $\text{C}_{60}$  interlayer between the  $\text{TiO}_2$  and the one-step-printed  $\text{MAPbI}_3$ , Liang et al. demonstrated a *PCE* of 17.0% for a 0.04  $\text{cm}^2$  solar cell and 13.3% for a 4  $\text{cm}^2$  (active area) PSC.<sup>[92]</sup> In the study of Li et al., only the  $\text{PbI}_2$  layers were inkjet-printed on mesoporous  $\text{TiO}_2$  and converted with MAI-powder into the perovskite. In this manner, large perovskite grains were obtained and the resulting solar cells showed a *PCE* of 18.6% for a 0.04  $\text{cm}^2$  large solar cell, and 17.7% for larger

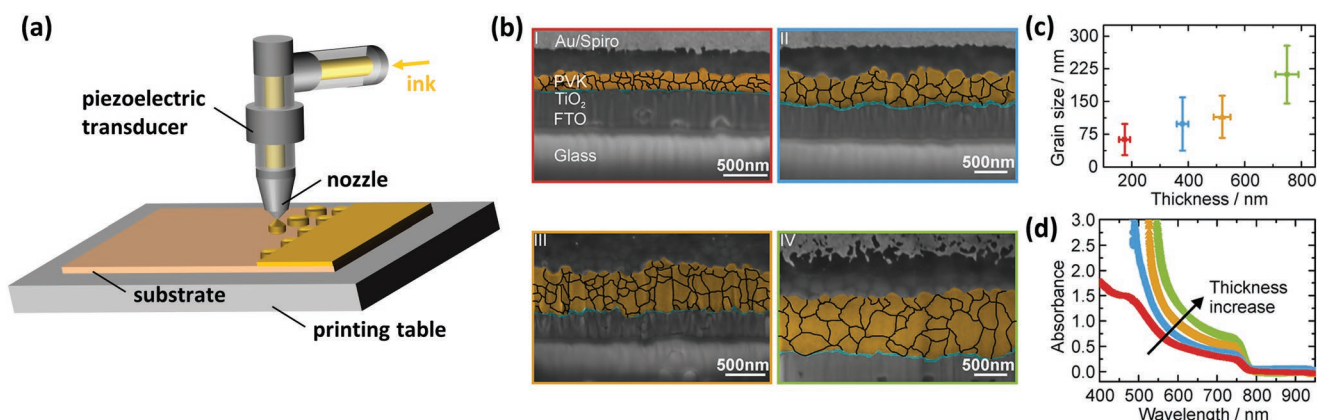


**Figure 3.** Inkjet printing. a) Schematic illustration of the inkjet printing process. b) Scanning electron microscopy (SEM) cross-sectional images of inkjet-printed multi-cation absorbers with different thicknesses. The crystallization dynamics, indicated in (c) through the measured grain size, is significantly influenced by the absorber thickness of the perovskite film, which, in turn, influences the optoelectronic properties of the perovskite films. b–d) Reproduced with permission.<sup>[91]</sup> Copyright 2108, the American Chemical Society.



(2 cm<sup>2</sup>) devices.<sup>[93]</sup> Recently, Schliske et al. demonstrated the flexibility of design that inkjet printing allows by printing arbitrary-shaped PSCs and also printing arbitrarily shaped luminescent down-shifting layers to realize different solar cell colors while maintaining a *PCE* of 9.5% for such devices.<sup>[94]</sup>

The increasing *PCE* of inkjet-printed PSCs demonstrates that the technology is becoming competitive with other deposition methods in terms of the quality of the active layer. Recently, Abzieher et al. demonstrated a *PCE* as high as 20.7% with a *V*<sub>OC</sub> of 1.11 V and fill factors (*FF*) above 80% with a printed multi-cation perovskite absorber in an architecture employing undoped electron-beam-evaporated NiO<sub>x</sub> as an HTL, and thermally evaporated C<sub>60</sub> and bathocuproine (BCP) as ETL.<sup>[95]</sup> Moreover, initial steps toward all inkjet printed PSC, wherein not just the perovskite layer is printed, were demonstrated. Recently, Huckaba et al. printed not only the perovskite layer but also a mesoporous TiO<sub>2</sub> and achieved 14.1% in *PCE*.<sup>[96]</sup> PSCs with printed WO<sub>x</sub> as ETL and printed spiro-OMeTAD as HTL have also been demonstrated, but to date showed only mediocre *PCE* (10.7%) with significant hysteresis.

To summarize, inkjet-printed perovskite absorber layers demonstrate comparable quality to other state-of-the-art PSCs, e.g., spin-coated devices, regarding *PCE* and stability. This advance has been achieved by attaining control of crystallization after printing by developing suitable perovskite inks, gas quenching, vacuum flash assisted solution processing (VASP) or annealing procedures. In comparison with other solution-based deposition techniques, it is hard to apply antisolvent techniques to control crystallization with an inkjet-printed approach. Some limitations and challenges remain for inkjet-printed PSC: although the printing procedure is very flexible regarding thickness and structure, the printing speed is limited by the numbers of nozzles and typically slower than other coating methods. Since the crystallization of perovskite is a (time-) critical process, this may lead to problems for the upscaling of the procedure, at least for commonly used inkjet printers on laboratory scale. Also, the development of suitable inks can be more difficult than for other coating techniques

since the exact wetting behavior of the ink is of key importance in inkjet printing.

### 2.3. Spray Coating

Spray coating is a solution-based deposition technique that is already widely used, for example, for automotive paintings. The advantages of low material wastage, high-throughput processing and roll-to-roll compatibility drew the attention of the perovskite scientific community to consider this technique for fabricating PSCs.<sup>[97,98]</sup>

A schematic of an ultrasonic spray coater is illustrated in Figure 4a. Typically, spray coaters use an ultrasonic tip vibrating at tens of kHz,<sup>[99,100]</sup> which creates a mist of ink droplets (or solvent mist) that are directed toward the substrate using a N<sub>2</sub> gas jet. Upon reaching the substrate, these droplets ideally merge and wet the substrate to create a continuous wet film that dries on the substrate. For the development of spray-coated PSCs, the first study was carried out by Barrows et al. in 2014, resulting in a *PCE* of 11.1%.<sup>[100]</sup> The work reported on important deposition parameters that affect the formation of the absorber layer: substrate temperature, volatility of the coating solvent and various post annealing temperatures. The study also showed that a moderate substrate temperature of ≈75 °C resulted in improved surface wetting and reduction of non-uniformities. In the following year, Ramesh et al. conducted a study using an airbrush pen to spray coat the perovskite precursor solutions.<sup>[101]</sup> In this study, PSCs with *PCE*s of up to 10.2% were demonstrated for small-area devices as well as first >3 cm<sup>2</sup> spray-coated perovskite devices with a more modest *PCE* of 4.5%. In 2016, Das et al. fabricated PSCs on flexible substrates with *PCE*s of 8.1%, showing for the first time the potential of roll-to-roll processing using spray-coated perovskite absorbers.<sup>[102]</sup> In the same year, Tait et al. reported the use of a concurrently pumped ultrasonic spray coater for the deposition of the perovskite layer.<sup>[99]</sup> This study demonstrated that using two separate inks mixed in variable ratios in the spray

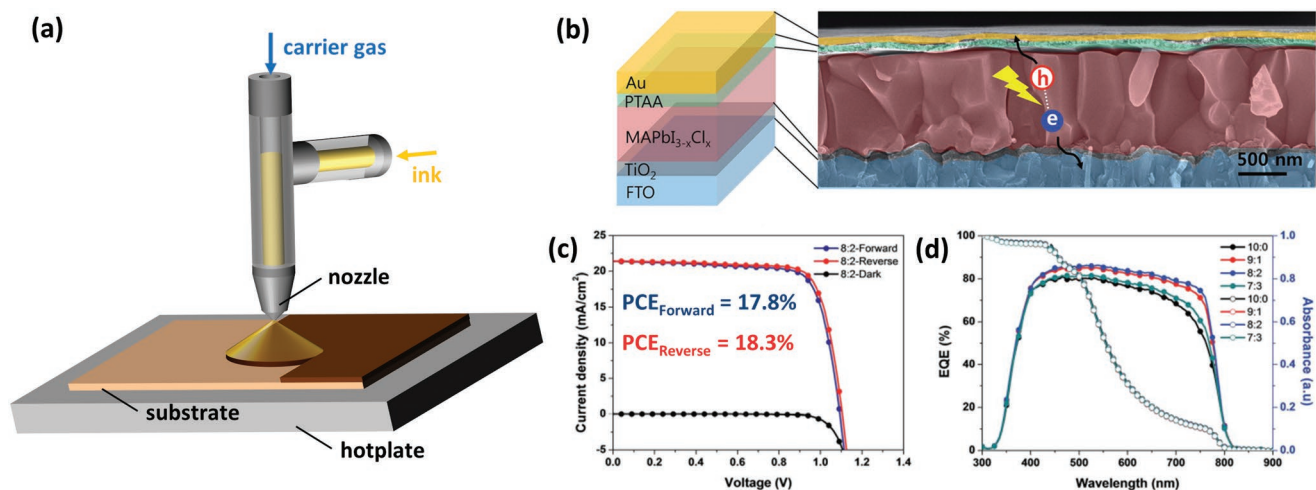


**Figure 4.** Spray coating. a) Schematic illustration of the spray coating process. b) SEM cross-sectional image of a high-quality spray-coated MAPbI<sub>3-x</sub>Cl<sub>x</sub> perovskite absorber. c) *PCE*s up to 18.3% in reverse *J*-*V* characteristics and d) high external quantum efficiency (EQE) were achieved, which is a result of a careful solvent engineering of the spray process. b–d) Reproduced with permission.<sup>[91]</sup> Copyright 2016, the Royal Society of Chemistry.

nozzle before aerosolization provide a robust method to perform compositional screening of perovskite materials.<sup>[99]</sup> The work demonstrated an improvement over the previous studies for both small-area PSCs and spray-coated perovskite PV modules, reaching efficiencies of 15.7% and 11.7% (3.8 cm<sup>2</sup>, aperture area) respectively.<sup>[99]</sup> Xia et al. demonstrated long-term stability of spray-coated PSCs via incorporating of Cs into the ink (12.5% PCE after 100 h of aging).<sup>[103]</sup> This confirmed the enhanced stability induced by inorganic Cs in multi-cation perovskites, which was also observed by Saliba et al. for spin-coated PSCs before.<sup>[8]</sup> Later, Hunag et al. increased the PCE of spray-coated PSCs to 16.0% with the use of a two-step spray-coating method for the absorber deposition.<sup>[104]</sup> In this method, the PbI<sub>2</sub> was first sprayed onto a heated substrate at 60 °C, then MAI was sprayed onto the dried film (heated to 80 °C). Finally, the resulting film was annealed between 100 and 115 °C (with an intermediate solvent wash) in order to convert the precursors and crystallize the perovskite thin-film. Very recently, Bishop et al. demonstrated spray-coated triple-cation perovskite using VASP. The method uses brief exposure to vacuum of the wet film after spraying in order to promote the formation of densely packed perovskite crystals and very smooth films (22 nm roughness). As a result, PCEs up to 17.8% were demonstrated for PSCs.<sup>[105]</sup> Heo et al. reported the highest PCE of 18.3% for spray-coated PSCs so far (see Figure 4b–d).<sup>[31]</sup> The study showed the significance of utilizing different boiling point solvents in various ratios to control the evaporation of solvents, but also relied on substrate heating at 120 °C.<sup>[31]</sup> As a result, large perovskite grains exhibiting a low number of trap states were demonstrated using solvent mixtures of DMF and GBL in a ratio of 8:2. Moreover, the fabrication of 100 cm<sup>2</sup> large PV modules with an active area of 40 cm<sup>2</sup> and a PCE of up to 15.5% was realized.<sup>[31]</sup> Recently, Uličná et al. reported the use of a slow-drying ink formulation that allowed an antisolvent approach to be used after spray coating. In this study, the ink contained slow-drying solvents that were extracted in an antisolvent diethylether bath. The solvent extraction in the antisolvent bath induced crystal nucleation, and a subsequent annealing at 150 °C promoted crystal growth, with the resulting devices reaching a maximum PCE of 17.3%.<sup>[106]</sup>

The previous studies mentioned above covered the spray coating of the absorber layer only. However, for an industrial roll-to-roll process, it is desired to also spray-coat the ETL and HTL and possibly even the electrodes. Several studies have already demonstrated this, for instance, spray coating of PEDOT:PSS,<sup>[107]</sup> CuSCN,<sup>[108]</sup> Spiro-OMeTAD,<sup>[109]</sup> compact TiO<sub>2</sub>,<sup>[8,109]</sup> mesoporous TiO<sub>2</sub>,<sup>[109]</sup> and PCBM.<sup>[110]</sup> Very recently, Mohamad et al. and Bishop et al. reported all-spray-coated PSCs.<sup>[109,110]</sup> Mohamad et al. used PEDOT:PSS and PCBM as their HTL and ETL, respectively, achieving 9.9% efficient devices<sup>[110]</sup> while, Bishop et al. achieved comparable device performance of 10.2% based on PSCs using spray-coated compact TiO<sub>2</sub>, mesoporous TiO<sub>2</sub> as ETLs and Spiro-OMeTAD as the HTL for their architecture.<sup>[109]</sup>

In summary, spray coating is a very suitable technique for upscaling the perovskite thin-films. By controlling the key process parameters, i.e., the precursor system, solvents, nozzle spray angle, the scanning speed, and the flow rate, a large process window for a high throughput fabrication of perovskite

thin-films as well as control over the quality of the perovskite thin-film is accessible.<sup>[97,98,100]</sup> The main challenges of this technique are crystal-growth related thickness variations,<sup>[100,109]</sup> solution de-wetting<sup>[100]</sup> and nonuniform substrate coverage<sup>[48,100,110]</sup> arising from the surface tension driven coffee-ring<sup>[111]</sup> or Marangoni effects.<sup>[112]</sup> However, these challenges can be tackled with a set of process control methods. First of all, optimization of the substrate temperature, the lateral head speed and head height, the solution concentration, and the fluid flow rate, allow for tuning of the wet film thickness and the drying rate. If the drying rate is too low or the wet film thickness is too large, the wet-film is subject to dewetting, the coffee-ring effect, and/or uncontrolled crystal growth. If however the drying rate is too high or the wet-film thickness too low, the droplets dry before coalescing and thereby yield an inhomogeneous layer with poor surface coverage.<sup>[99,100,109,110]</sup> Beyond control of process parameters, ink formulations using solvent mixtures and additives have been critical in addressing these issues.<sup>[31,109,110]</sup>

#### 2.4. Screen Printing, Relief Printing, and Gravure Printing

The deposition of patterned perovskite layers may be attractive, and this can be approached by inkjet printing.<sup>[32,91]</sup> However, traditional technologies like screen printing, gravure printing, and relief printing (flexography) are often the first choice in industry when printing of defined areas or patterns is needed. These three techniques have in common that the image to be printed first has to be engraved onto an image carrier before it is transferred onto the substrate (see Figure 5a–c). In case of screen printing, the image carrier is a mesh equipped with a stencil defining the printing pattern. For gravure and relief printing, a cylindrical image carrier is used. In case of gravure printing the (periodic) image is engraved into the printing cylinder and filled with the ink. Relief printing is based on the same principle; however, the image on the printing cylinder is not engraved but a relief structure.

In the field of PSCs, screen printing is widely used for the deposition of HTL, ETL, and contact layers. Mesoporous transport layers are deposited successfully by screen printing in various groups, with mesoporous TiO<sub>2</sub> being the most studied material.<sup>[71,90,113–118]</sup> Indeed, the first demonstrated PSC demonstrated by Kojima et al. in 2009 was equipped with a screen-printed mesoporous TiO<sub>2</sub> layer, which was prepared from a commercially available nanocrystalline TiO<sub>2</sub> paste sintered above 400 °C.<sup>[119]</sup> By doing so, up to 12 μm thick mesoporous TiO<sub>2</sub> layers could be demonstrated, acting as an efficient ETL in a 3.8% efficient device.<sup>[119]</sup> From that point on, other oxides like Al<sub>2</sub>O<sub>3</sub>,<sup>[117,120]</sup> ZrO<sub>2</sub>,<sup>[90,113,116,118,121]</sup> and NiO<sup>[117,120]</sup> have been deposited by screen printing as well. High quality printable mesoporous oxide layers are of key importance for fully printable PSCs as the crystallization of the perovskite absorber is controlled by the scaffold of the underlying charge transport material. In this regard, screen printing of mesoporous oxides as supporting host layer is considered to be a promising way of controlling the crystallization in fully printed perovskite solar cells.<sup>[35]</sup> In 2013, Ku et al. reported on a screen-printed multilayer sequence using a 1 μm thick TiO<sub>2</sub> ETL, a 1 μm thick ZrO<sub>2</sub> spacer layer, and a 10 μm thick carbon layer acting as the



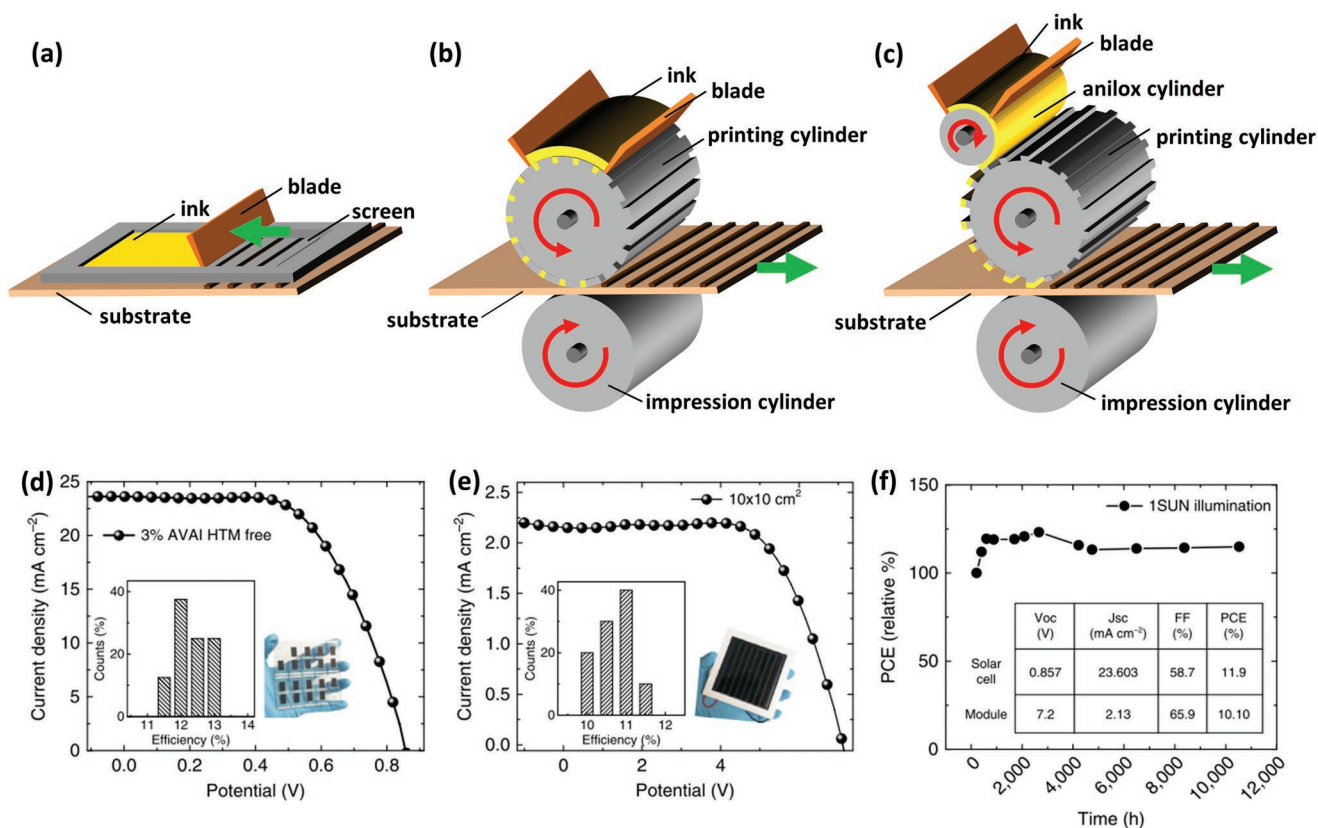


**Figure 5.** Screen printing, gravure printing, and relief printing. a–c) Schematic illustration of screen printing (a), gravure printing (b), and relief printing (c) processes. d,e) The performance of all-printed PSCs (d) and all-printed perovskite PV modules (e) with screen-printed mesoporous TiO<sub>2</sub> charge transport layers and carbon back electrodes. f) In addition, a stable power output for more than a year is demonstrated. d–f) Adapted with permission.<sup>[124]</sup> Copyright 2017, Springer Nature.

back electrode of the device.<sup>[113]</sup> For the first time, this approach allowed a fully printed, HTL-free PSC with a *PCE* of up to 6.6%. Using a similar approach, Mei et al. demonstrated a novel absorber infiltrated into the screen-printed layer stack, resulting in solar cells with *PCEs* above 12.0% and a stability of >1000 h in ambient air under one-sun illumination.<sup>[121]</sup> The high stability in ambient and humid environments in these devices is commonly explained by the hydrophobic nature of the carbon back electrode, functioning as a water protective layer.<sup>[122]</sup> By optimizing the layer stack, the *PCE* was improved to 14.0% for small-area devices as reported in 2017.<sup>[123]</sup> More importantly, upscaling of the fully printable process was shown and PV mini-modules consisting of ten monolithically interconnected subcells on a 10 × 10 cm<sup>2</sup> substrate with *PCEs* over 10% (active area 49 cm<sup>2</sup>) were achieved, along with a first large (7 m<sup>2</sup>) prototype PV panel.<sup>[123]</sup> The *PCE* of the fully printable PV modules could be further improved to 11.2% (46.7 cm<sup>2</sup>, active area) with an extraordinary stability of >10 000 h at 55 °C under air-mass 1.5 global (AM1.5G) illumination (see Figure 5d–f).<sup>[124]</sup> Since then, the approach was further optimized, with *PCEs* of up to 15.6% being realized for small-area screen-printed devices.<sup>[118]</sup> However, this increase is attributed to an improved composition of the perovskite layer by using novel bifunctional conjugated organic cations, rather than the printing method itself.<sup>[118]</sup>

In summary, screen-printing is an effective process for creating mesoporous scaffolds with micron-scale thicknesses that

can then control the nucleation and crystallization perovskite absorbers infiltrated into them. In contrast to other coating and printing techniques, the quality of the mesoporous scaffolds is the key element to control the morphology of the perovskite absorber layer, rather than the deposition parameters of the perovskite precursor inks themselves. Screen printing is a promising candidate for industrial-scale fabrication of fully printed perovskite PV modules, combining the potential of very low production costs (capital expenditure and running costs) with a high throughput. However, a key limitation is its reliance on mesoporous layer architectures, these necessitate processes above 400 °C and could add unique challenges for achieving high *PCEs*.

On the pathway toward mass production of perovskite PV modules, gravure and relief printing might be of special interest for scalable roll-to-roll fabrication. However, in contrast to OPV, where gravure printing is frequently used for the deposition of patterned structures in PV modules,<sup>[125,126]</sup> these techniques are less-studied for PSCs. So far, gravure printing of perovskites has only been used by Hu et al., who reported highly oriented perovskite nanowires fabricated by a roll-to-roll microengraving process on flexible polyethylene terephthalate (PET) foil.<sup>[127]</sup> Particularly, it is suggested that the combination of coating and printing techniques employing cylindrical image carriers and screen printing (known as rotary screen printing) should be researched for perovskite-based devices, as this

might open up new possibilities in terms of an industrialized roll-to-roll fabrication.

### 3. State-of-the-Art Results

With state-of-the-art *PCEs* exceeding 22% for spin-coated PSCs (current record *PCE* is 23.7%),<sup>[1]</sup> the *PCEs* of PSCs processed by scalable solution-based deposition techniques discussed herein, lag a few years behind the small-area spin-coated state-of-the-art. Nonetheless, the various successful demonstrations of high *PCEs* inspires confidence that with further engineering and optimization the *PCEs* of PSCs processed from scalable solution-based deposition techniques will soon approach the state-of-the-art spin-coated records. In **Figure 6a** and **Table 1**, the recent achievements in terms of coating method, *PCEs* taken from *J–V*-characteristics, and solar cell area are summarized. A more detailed tabular summary including more figures-of-merit, and notes on the solar cell structure and details of the deposition method can be found in the Supplementary Information. For several of the discussed scalable solution-based deposition techniques (blade coating, slot-die coating, inkjet printing, and spray coating), the first studies already date back around 5 years. Subsequently, these techniques demonstrated a steep learning curve and reached *PCEs* >17.5%, even if still only on small areas. Comparing these values to the evolution of the *PCEs* of state-of-the-art spin-coated PSCs, it is estimated that the development of scalable solution-based deposition techniques lags around 3–4 years behind the laboratory-scale spin-coating technique.

While the intrinsic material stability and device stability toward moisture, oxygen, temperature, and light is not expected to be different for scalable solution-based deposition techniques, the stable power output of PSC is known to depend strongly on the fabrication of the perovskite thin-film absorber layer.<sup>[99]</sup> Hysteresis in *J–V* measurements is a commonly reported issue, which impedes a proper determination of the *PCE* by *J–V* characteristics.<sup>[128]</sup> For this purpose, a second more trustworthy route to determine the *PCE* is established in

the field. In addition to the *PCE* derived from *J–V* measurements, researchers also report the stable power output efficiency. The stable power output efficiency is generally denoted as the power output tracked under constant voltage or even maximum power point tracking of the PSC under AM1.5G illumination for 30 s to 10 min (large variation in tracking time due to a lack of standardized test protocols). For the state-of-the-art PSCs fabricated with spin coating the stable power output efficiency is nowadays almost identical to the *PCE* determined from *J–V* measurements.<sup>[129]</sup> However, for less efficient devices and those that exhibit a strong hysteresis, these values can differ strongly. With regard to the scalable solution-based deposition techniques reported in this work, the stable power output efficiencies still lag further behind the reported *PCEs* from *J–V* measurements (see Table S1, Supporting Information). The highest reported stable power output efficiencies are mostly <16%—with slot-die coating: 15.4%;<sup>[73]</sup> spray coating: 17.0%;<sup>[105]</sup> inkjet printing: 18.5%;<sup>[95]</sup> and screen printing: 14.6%;<sup>[124]</sup> indicating that the perovskite layers deposited by these techniques still have not yet reached the same homogeneity and quality of perovskite thin-films as the spin-coated reference devices. In particular, the discrepancy between the *PCE* determined from *J–V* measurements and the stable power output efficiency for printed or coated perovskite films indicates that improvements in the perovskite film formation over large areas—likely the uniform control of perovskite nucleation and crystallization—and interfaces are still required.

Next to the *PCE*, the device area is an essential measure of the progress of scalable solution-based deposition techniques. In **Figure 6b**, this progress is shown for the coating and printing techniques discussed in this work. While for small-area solar cells the definition of the device area is univocal, the *PCE* of perovskite PV modules is not reported consistently in literature. From an application perspective the *PCE* should be reported with respect to the aperture area, but in several early studies the *PCE* is provided with regard to the active area instead. In order to provide a consistent summary of the performance development during upscaling, aperture areas of the solar modules (partly calculated based on reported geometrical

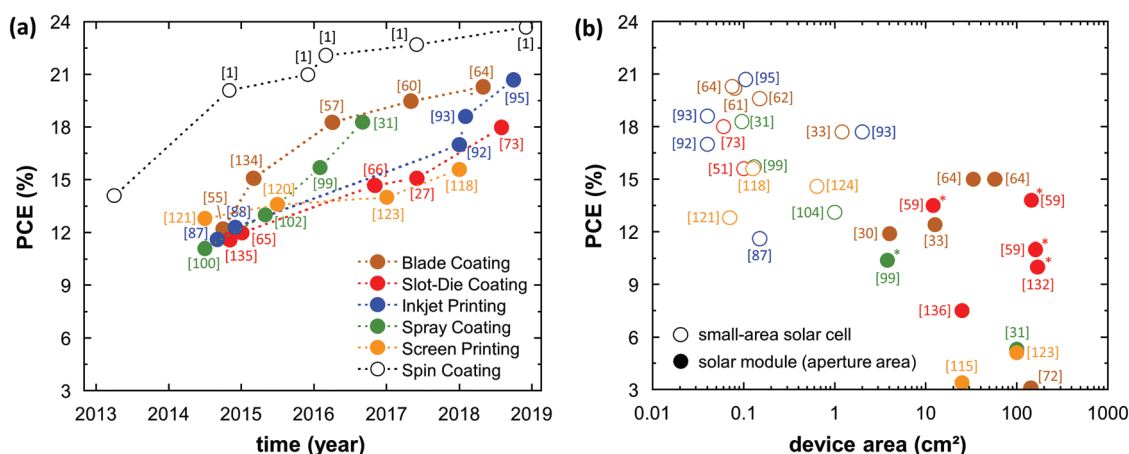


**Figure 6.** a) Chronological evolution of *PCEs* determined by *J–V*-measurements (different device areas) (see refs.: [1,27,31,55,57,60,61,64-66,73,87,88,92,93,95,99,100,102,105,118,120,121,123,130,131,134,135]) and b) distribution of the *PCEs* of PSCs and PV modules in terms of the device area fabricated with different printing or coating techniques (see refs.: [30,31,33,51,59,61,62,64,72,73,87,92,93,95,99,104,115,118,121,123,125,132,136]). For the PV modules, aperture areas are used in order to give a consistent overview. Points marked by \* are stabilized *PCEs*.

**Table 1.** Highest reported PCEs derived from  $J-V$  measurements and corresponding stabilized power output efficiency of PSCs via a range of coating techniques.

| Coating Technique | Year | PCE from $J-V$ [%]<br>(area [cm <sup>2</sup> ]) | Stabilized power output efficiency [%] | Material   | Ref.  |
|-------------------|------|---|--|--|-------|
| Spin Coating      | 2018 | 23.7 (n.a.)                                     | n.a.                                   | n.a. <sup>a)</sup>   | [1]   |
| Spin Coating      | 2018 | 23.2 (0.094)                                    | 22.9                                   | (FAPbI <sub>3</sub> ) <sub>0.95</sub> (MAPbBr <sub>3</sub> ) <sub>0.05</sub>   | [130] |
| Blade Coating     | 2018 | 20.3 (0.075)                                    | n.a.                                   | CH <sub>3</sub> NH <sub>3</sub> PbI <sub>3</sub>   | [64]  |
| Blade Coating     | 2018 | 20.2 (0.08)                                     | 19.9                                   | CH <sub>3</sub> NH <sub>3</sub> PbI <sub>3</sub>   | [61]  |
| Slot-Die Coating  | 2018 | 18.0 (0.06)                                     | 15.7                                   | CH <sub>3</sub> NH <sub>3</sub> PbI <sub>3-x</sub> Cl <sub>x</sub>   | [73]  |
| Slot-Die Coating  | 2018 | 18.3 (0.1)                                      | n.a.                                   | CH <sub>3</sub> NH <sub>3</sub> PbI <sub>3-x</sub> Cl <sub>x</sub>   | [131] |
| Slot-Die Coating  | 2018 | 17.4 (0.06)                                     | 14.2                                   | CH <sub>3</sub> NH <sub>3</sub> PbI <sub>3-x</sub> Cl <sub>x</sub>   | [132] |
| Spray Coating     | 2016 | 18.3 (0.1)                                      | n.a.                                   | CH <sub>3</sub> NH <sub>3</sub> PbI <sub>3-x</sub> Cl <sub>x</sub>   | [31]  |
| Spray Coating     | 2018 | 17.8 (0.03)                                     | 17.0                                   | Cs <sub>1.05</sub> ((FAPbI <sub>3</sub> ) <sub>0.85</sub> (MAPbBr <sub>3</sub> ) <sub>0.15</sub> ) <sub>0.95</sub>               | [105] |
| Inkjet Printing   | 2018 | 18.6 (0.04)                                     | 18.3                                   | CH <sub>3</sub> NH <sub>3</sub> PbI <sub>3</sub>   | [93]  |
| Inkjet Printing   | 2018 | 20.7 (0.105)                                    | 18.5                                   | Cs <sub>0.1</sub> (FA <sub>0.83</sub> MA <sub>0.17</sub> ) <sub>0.9</sub> Pb(Br <sub>0.17</sub> I <sub>0.83</sub> ) <sub>3</sub> | [95]  |
| Screen Printing   | 2018 | 15.6 (0.126)                                    | 15.4                                   | (AB) <sub>2</sub> (MA) <sub>49</sub> Pb <sub>50</sub> I <sub>151</sub> <sup>b)</sup>   | [118] |

<sup>a)</sup>No information provided from NREL; <sup>b)</sup>AB: bifunctional conjugated organic molecule 4-(aminomethyl) benzoic acid hydroiodide.

fill factors) are used in Figure 6b. All scalable coating and printing methods showed notable progress in upscaling to larger area devices over the past few years. Fully printed or coated PV modules with active areas larger than 100 cm<sup>2</sup> and PCEs above 10% were demonstrated.<sup>[123,132]</sup> Moreover, for almost all scalable solution-based deposition techniques discussed here, already today fully interconnected PV modules have been demonstrated with scalable interconnection schemes and stable power output of PCE >11%—for example, slot-die coating: 13.8% (144 cm<sup>2</sup>, aperture area);<sup>[74]</sup> blade coating: 14.6% (57 cm<sup>2</sup>, aperture area);<sup>[64]</sup> spray coating: 15.5% (40 cm<sup>2</sup>, active area);<sup>[31]</sup> and screen printing: 10.4% (49 cm<sup>2</sup>, active area).<sup>[123]</sup> Since these values are comparable or and mostly even exceed the highest certified PCEs reported for perovskite PV (including spin coated perovskite absorber layers) of this area (PCE of 16.5%, designated area >16.3 cm<sup>2</sup>),<sup>[133]</sup> the general scalability of perovskite PV based on the solution-based deposition techniques discussed in this work is demonstrated—with excellent results for slot-die coating and blade coating in particular. However, the PCE gap between small- and large-area devices is still enormous, reflecting the yet poor control of the perovskite thin-film homogeneity. Therefore, extensive future research and development is needed to control the quality of coated or printed perovskite materials over larger areas.

Given the rapid progress in achieving good material quality and the similar learning curves evident in Figure 6a, all of the coating and printing techniques (with the exception of screen printing) appear capable of being developed to deliver good quality active-layer materials over large areas. The decision with regard to which technique or techniques may ultimately be used in industrial production will be made based on total cost considerations. Given the uncertainty as to how other layers will be deposited, and the exact mechanism each of the coating/printing methods will ultimately use to control crystallization no meaningful prediction of these can yet be made. For these reasons, we recommend further parallel competition between concurrent scientific investigations of all the reviewed methods.

## 4. Conclusion and Outlook

In summary, impressive progress has been made in the last few years on producing perovskite PV using scalable printing and coating technologies. Multiple of these techniques produce solar cells lagging behind the best spin-coated solar cells by less than 5% in terms of power conversion efficiency for small-area solar cells. The key developments that have enabled this rapid progress in coated and printed PSCs are the control of nucleation and crystal growth of the perovskite crystal structure. The progress in literature to date suggests that such control is well achieved in the simpler one-step deposition route, wherein all precursors are introduced in a single coating or printing step. Engineering of the ink to allow a slow drying and processing time window sufficiently long for subsequent nonsolvent treatment appears to be a promising route to eventually reproduce the quality of the best spin-coated perovskite thin-films in a variety of coating and printing techniques. However, this does carry the disadvantage of requiring the addition of a nonsolvent treatment into the process chain. Therefore, the continued investigation of other techniques to induce nucleation and control crystal growth, such as gas quenching, vacuum induced crystallization, and elevated substrate temperatures (in combination with appropriate ink engineering) remains of great relevance and is likely to ultimately lead to scalable high-quality PSCs. Besides the challenge of closing the efficiency gap between small-area solar cells and large-area PV modules, a key challenge, and major research priority is to improve the uniformity of the quality of printed perovskites over larger areas. This will be essential in order to enable commercial perovskite PV modules with active areas above 1 m<sup>2</sup>.

## Acknowledgements

The authors are grateful to the great spirit of the taskforce “Perovskite Photovoltaics” at KIT and the scientific discussions with the group of



Willi Schabel (TVT KIT). The financial support by the Federal Ministry for Research and Education (BMBF) through the projects PRINTPERO (03SF0557A) and PeroSol, the Initiating and Networking Funding of the Helmholtz Association (HYIG of U.W.P. (VH-NG-1148); Recruitment Initiative of B.S.R.; the Helmholtz Energy Materials Foundry (HEMF); PEROSEED (ZT-0024); and the Science and Technology of Nanostructures Research Programme) as well as the Karlsruhe School of Optics & Photonics (KSOP) is gratefully acknowledged.

## Conflict of Interest

The authors declare no conflict of interest.

## Keywords

coating, metal halide perovskites solar cells, printing, solution-processed photovoltaics, upscaling

Received: October 16, 2018

Revised: January 23, 2019

Published online:

- [1] NREL, "NREL Efficiency Chart," <https://www.nrel.gov/pv/assets/pdfs/best-research-cell-efficiencies.20190327.pdf> (accessed: March 2019).
- [2] S. D. Stranks, G. E. Eperon, G. Grancini, C. Menelaou, M. J. P. Alcocer, T. Leijtens, L. M. Herz, A. Petrozza, H. J. Snaith, *Science* **2013**, *342*, 341.
- [3] S. De Wolf, J. Holovsky, S.-J. Moon, P. Löper, B. Niesen, M. Ledinsky, F.-J. Haug, J.-H. Yum, C. Ballif, *J. Phys. Chem. Lett.* **2014**, *5*, 1035.
- [4] Z. Li, Y. Zhao, X. Wang, Y. Sun, Z. Zhao, Y. Li, H. Zhou, Q. Chen, *Joule* **2018**, *2*, 1559.
- [5] G. E. Eperon, S. D. Stranks, C. Menelaou, M. B. Johnston, L. M. Herz, H. J. Snaith, *Energy Environ. Sci.* **2014**, *7*, 982.
- [6] S. Christodoulou, F. Di Stasio, S. Pradhan, A. Stavrinadis, G. Konstantatos, *J. Phys. Chem. C* **2018**, *122*, 7621.
- [7] M. Jaysankar, W. Qiu, J. Bastos, J. G. Tait, M. Debucquoy, U. W. Paetzold, D. Cheyns, J. Poortmans, *J. Mater. Chem. A* **2016**, *4*, 10524.
- [8] M. Saliba, T. Matsui, J.-Y. Seo, K. Domanski, J.-P. Correa-Baena, M. K. Nazeeruddin, S. M. Zakeeruddin, W. Tress, A. Abate, A. Hagfeldt, M. Grätzel, *Energy Environ. Sci.* **2016**, *9*, 1989.
- [9] M. Saliba, T. Matsui, K. Domanski, J. Y. Seo, A. Ummadisingu, S. M. Zakeeruddin, J. P. Correa-Baena, W. R. Tress, A. Abate, A. Hagfeldt, M. Grätzel, *Science* **2016**, *354*, 206.
- [10] T. Duong, Y. L. Wu, H. Shen, J. Peng, X. Fu, D. Jacobs, E. C. Wang, T. C. Kho, K. C. Fong, M. Stocks, E. Franklin, A. Blakers, N. Zin, K. McIntosh, W. Li, Y. B. Cheng, T. P. White, K. Weber, K. Catchpole, *Adv. Energy Mater.* **2017**, *7*, 1700228.
- [11] D. P. McMeekin, G. Sadoughi, W. Rehman, G. E. Eperon, M. Saliba, M. T. Horantner, A. Haghighirad, N. Sakai, L. Korte, B. Rech, M. B. Johnston, L. M. Herz, H. J. Snaith, *Science* **2016**, *351*, 151.
- [12] J. S. Manser, M. I. Saidaminov, J. A. Christians, O. M. Bakr, P. V. Kamat, *Acc. Chem. Res.* **2016**, *49*, 330.
- [13] Q. Fu, X. Tang, B. Huang, T. Hu, L. Tan, L. Chen, Y. Chen, *Adv. Sci.* **2018**, *5*, 1700387.
- [14] G. Niu, X. Guo, L. Wang, *J. Mater. Chem. A* **2015**, *3*, 8970.
- [15] B. Salhi, Y. S. Wudil, M. K. Hossain, A. Al-Ahmed, F. A. Al-Sulaiman, *Renewable Sustainable Energy Rev.* **2018**, *90*, 210.
- [16] X. Qin, Z. Zhao, Y. Wang, J. Wu, Q. Jiang, J. You, *J. Semicond.* **2017**, *38*, 011002.
- [17] D. Li, P. Liao, X. Shai, W. Huang, S. Liu, H. Li, Y. Shen, M. Wang, *RSC Adv.* **2016**, *6*, 89356.
- [18] Q. Zhang, F. Hao, J. Li, Y. Zhou, Y. Wei, H. Lin, *Sci. Technol. Adv. Mater.* **2018**, *19*, 425.
- [19] P. V. Kamat, J. Bisquert, J. Buriak, *ACS Energy Lett.* **2017**, *2*, 904.
- [20] S. Yang, W. Fu, Z. Zhang, H. Chen, C. Z. Li, *J. Mater. Chem. A* **2017**, *5*, 11462.
- [21] M. Lee, K. Lu, Y. Chen, K. Lin, W. Chen, T. Chen, K. Chen, H. Lu, Y. Lin, D. Walker, M. Creally, G. Béalle, H. Wang, H. Tseng, M. Goulding, E. Boehm, H. Buchholz, *SID Symp. Dig. Tech. Pap.* **2018**, *49*, 624.
- [22] E. Böhm, P. Levermore, H. Tseng, G. Bealle, H. Wang, P. Hibon, H. Heil, A. Jatsch, H. Buchholz, M. Kga, F. Strasse, *SID Symp. Dig. Tech. Pap.* **2017**, *48*, 842.
- [23] J. E. Carlé, M. Helgesen, O. Hagemann, M. Hösel, I. M. Heckler, E. Bundgaard, S. a. Gevorgyan, R. R. Søndergaard, M. Jørgensen, R. García-Valverde, S. Chaouki-Almagro, J. a. Villarejo, F. C. Krebs, *Joule* **2017**, *1*, 274.
- [24] J. Ávila, C. Momblona, P. P. Boix, M. Sessolo, H. J. Bolink, *Joule* **2017**, *1*, 431.
- [25] F. C. Krebs, *Sol. Energy Mater. Sol. Cells* **2009**, *93*, 394.
- [26] J. J. van Franeker, K. H. Hendriks, B. J. Bruijnaers, M. W. G. M. Verhoeven, M. M. Wienk, R. a. J. Janssen, *Adv. Energy Mater.* **2017**, *7*, 1601822.
- [27] Q. Hu, L. Zhao, J. Wu, K. Gao, D. Luo, Y. Jiang, Z. Zhang, C. Zhu, E. Schaible, A. Hexemer, C. Wang, Y. Liu, W. Zhang, M. Grätzel, F. Liu, T. P. Russell, R. Zhu, Q. Gong, *Nat. Commun.* **2017**, *8*, 1.
- [28] W. Qiu, T. Merckx, M. Jaysankar, C. Masse De La Huerta, L. Rakocevic, W. Zhang, U. W. Paetzold, R. Gehlhaar, L. Froyen, J. Poortmans, D. Cheyns, H. J. Snaith, P. Heremans, *Energy Environ. Sci.* **2016**, *9*, 484.
- [29] N.-G. Park, *CrystEngComm* **2016**, *18*, 5977.
- [30] K. L. Gardner, J. G. Tait, T. Merckx, W. Qiu, U. W. Paetzold, L. Kootstra, M. Jaysankar, R. Gehlhaar, D. Cheyns, P. Heremans, J. Poortmans, *Adv. Energy Mater.* **2016**, *6*, 1600386.
- [31] J. H. Heo, M. H. Lee, M. H. Jang, S. H. Im, *J. Mater. Chem. A* **2016**, *4*, 17636.
- [32] F. Mathies, T. Abzieher, A. Hochstuhl, K. Glaser, A. Colsmann, U. W. Paetzold, G. Hernandez-Sosa, U. Lemmer, A. Quintilla, *J. Mater. Chem. A* **2016**, *4*, 19207.
- [33] M. Yang, Z. Li, M. O. Reese, O. G. Reid, D. H. Kim, S. Siol, T. R. Klein, Y. Yan, J. J. Berry, M. F. A. M. van Hest, K. Zhu, *Nat. Energy* **2017**, *2*, 17038.
- [34] F. Ye, H. Chen, F. Xie, W. Tang, M. Yin, J. He, E. Bi, Y. Wang, X. Yang, L. Han, *Energy Environ. Sci.* **2016**, *9*, 2295.
- [35] G. E. Eperon, V. M. Burlakov, P. Docampo, A. Goriely, H. J. Snaith, *Adv. Funct. Mater.* **2014**, *24*, 151.
- [36] Y. Jo, K. S. Oh, M. Kim, K. H. Kim, H. Lee, C. W. Lee, D. S. Kim, *Adv. Mater. Interfaces* **2016**, *3*, 1.
- [37] T. Abzieher, F. Mathies, M. Hetterich, A. Welle, D. Gerthsen, U. Lemmer, U. W. Paetzold, M. Powalla, *Phys. Status Solidi A* **2017**, *214*, 1700509.
- [38] D.-Y. Son, S.-G. Kim, J.-Y. Seo, S.-H. Lee, H. Shin, D. Lee, N.-G. Park, *J. Am. Chem. Soc.* **2018**, *140*, 1358.
- [39] W. Zhang, S. Pathak, N. Sakai, T. Stergiopoulos, P. K. Nayak, N. K. Noel, A. a. Haghighirad, V. M. Burlakov, D. W. Dequillettes, A. Sadhanala, W. Li, L. Wang, D. S. Ginger, R. H. Friend, H. J. Snaith, *Nat. Commun.* **2015**, *6*, 10030.
- [40] T. Li, Y. Pan, Z. Wang, Y. Xia, Y. Chen, W. Huang, *J. Mater. Chem. A* **2017**, *5*, 12602.
- [41] J.-H. Im, I.-H. Jang, N. Pellet, M. Grätzel, N.-G. Park, *Nat. Nanotechnol.* **2014**, *9*, 927.

- [42] N. J. Jeon, J. H. Noh, Y. C. Kim, W. S. Yang, S. Ryu, S. Il Seok, *Nat. Mater.* **2014**, *13*, 897.
- [43] K. M. Lee, C. J. Lin, B. Y. Liou, S. M. Yu, C. C. Hsu, V. Suryanarayanan, M. C. Wu, *Sol. Energy Mater. Sol. Cells* **2017**, *172*, 368.
- [44] M. Saliba, J. P. Correa-Baena, C. M. Wolff, M. Stollerfoht, N. Phung, S. Albrecht, D. Neher, A. Abate, *Chem. Mater.* **2018**, *30*, 4193.
- [45] X. Li, D. Bi, C. Yi, J. D. Décoppet, J. Luo, S. M. Zakeeruddin, A. Hagfeldt, M. Grätzel, *Science* **2016**, *353*, 58.
- [46] A. Babayigit, J. D'Haen, H. G. Boyen, B. Conings, *Joule* **2018**, *2*, 1205.
- [47] B. Conings, A. Babayigit, M. T. Klug, S. Bai, N. Gauquelin, N. Sakai, J. T. W. Wang, J. Verbeeck, H. G. Boyen, H. J. Snaith, *Adv. Mater.* **2016**, *28*, 10701.
- [48] M. Remeika, S. R. Raga, S. Zhang, Y. Qi, *J. Mater. Chem. A* **2017**, *5*, 5709.
- [49] L. L. Gao, K. J. Zhang, N. Chen, G. J. Yang, *J. Mater. Chem. A* **2017**, *5*, 18120.
- [50] L. L. Gao, C. X. Li, C. J. Li, G. J. Yang, *J. Mater. Chem. A* **2017**, *5*, 1548.
- [51] C. Zuo, D. Vak, D. Angmo, L. Ding, M. Gao, *Nano Energy* **2018**, *46*, 185.
- [52] Z. Yang, C.-C. Chueh, F. Zuo, J. H. Kim, P.-W. Liang, A. K.-Y. Jen, *Adv. Energy Mater.* **2015**, *5*, 1500328.
- [53] G. W. Kim, D. V. Shinde, T. Park, *RSC Adv.* **2015**, *5*, 99356.
- [54] H. Back, J. Kim, G. Kim, T. Kyun Kim, H. Kang, J. Kong, S. Ho Lee, K. Lee, *Sol. Energy Mater. Sol. Cells* **2016**, *144*, 309.
- [55] J. H. Kim, S. T. Williams, N. Cho, C.-C. Chueh, A. K.-Y. Jen, *Adv. Energy Mater.* **2015**, *5*, 1401229.
- [56] Q. Wang, M. Eslamian, T. Zhao, A. K.-Y. Jen, *IEEE J. Photovoltaics* **2018**, *8*, 1662.
- [57] Y. Deng, Q. Dong, C. Bi, Y. Yuan, J. Huang, *Adv. Energy Mater.* **2016**, *6*, 1600372.
- [58] Y.-J. Heo, J.-E. Kim, H. Weerasinghe, D. Angmo, T. Qin, K. Sears, K. Hwang, Y.-S. Jung, J. Subbiah, D. J. Jones, M. Gao, D.-Y. Kim, D. Vak, *Nano Energy* **2017**, *41*, 443.
- [59] F. Di Giacomo, H. Fledderus, H. Gorter, G. Kirchner, I. De Vries, I. Dogan, W. Verhees, V. Zardetto, M. Najafi, D. Zhang, H. Lifka, Y. Galagan, S. Veenstra, P. Groen, R. Andriessen, *RESPECT 2018 Proc.*, IEEE, Piscataway, NJ, USA **2018**, p. 2795.
- [60] S. Tang, Y. Deng, X. Zheng, Y. Bai, Y. Fang, Q. Dong, H. Wei, J. Huang, *Adv. Energy Mater.* **2017**, *7*, 1700302.
- [61] W.-Q. Wu, Q. Wang, Y. Fang, Y. Shao, S. Tang, Y. Deng, H. Lu, Y. Liu, T. Li, Z. Yang, A. Gruverman, J. Huang, *Nat. Commun.* **2018**, *9*, 1625.
- [62] B. Dou, J. B. Whitaker, K. Bruening, D. T. Moore, L. M. Wheeler, J. Ryter, N. J. Breslin, J. J. Berry, S. M. Garner, F. S. Barnes, S. E. Shaheen, C. J. Tassone, K. Zhu, M. F. A. M. van Hest, *ACS Energy Lett.* **2018**, *3*, 2558.
- [63] D. Lee, Y.-S. S. Jung, Y.-J. Heo, S. Lee, K. Hwang, Y.-J. Jeon, J.-E. E. Kim, J. Park, G. Y. Jung, D.-Y. Y. Kim, *ACS Appl. Mater. Interfaces* **2018**, *10*, 16133.
- [64] Y. Deng, X. Zheng, Y. Bai, Q. Wang, J. Zhao, J. Huang, *Nat. Energy* **2018**, *3*, 560.
- [65] K. Hwang, Y. S. Jung, Y. J. Heo, F. H. Scholes, S. E. Watkins, J. Subbiah, D. J. Jones, D. Y. Kim, D. Vak, *Adv. Mater.* **2015**, *27*, 1241.
- [66] D. Burkitt, J. Searle, T. Watson, *R. Soc. Open Sci.* **2018**, *5*, 172158.
- [67] T. Qin, W. Huang, J. E. Kim, D. Vak, C. Forsyth, C. R. McNeill, Y. B. Cheng, *Nano Energy* **2017**, *31*, 210.
- [68] Y. Galagan, F. Di Giacomo, H. Gorter, G. Kirchner, I. de Vries, R. Andriessen, P. Groen, *Adv. Energy Mater.* **2018**, *8*, 1801935.
- [69] Y.-S. S. Jung, K. Hwang, Y.-J. Heo, J.-E. E. Kim, D. Lee, C.-H. H. Lee, H.-I. I. Joh, J.-S. S. Yeo, D.-Y. Y. Kim, *ACS Appl. Mater. Interfaces* **2017**, *9*, 27832.
- [70] J. Ciro, M. A. Mejía-Escobar, F. Jaramillo, *Sol. Energy* **2017**, *150*, 570.
- [71] T. M. Schmidt, T. T. Larsen-Olsen, J. E. Carlé, D. Angmo, F. C. Krebs, *Adv. Energy Mater.* **2015**, *5*, 1500569.
- [72] S. Razza, F. Di Giacomo, F. Matteocci, L. Cinà, A. L. Palma, S. Casaluci, P. Cameron, A. D'Epifanio, S. Licocchia, A. Reale, T. M. Brown, A. Di Carlo, *J. Power Sources* **2015**, *277*, 286.
- [73] J. B. Whitaker, D. H. Kim, B. W. Larson, F. Zhang, J. J. Berry, M. F. A. M. van Hest, K. Zhu, *Sustainable Energy Fuels* **2018**, *2*, 2442.
- [74] PV-Magazine, "Solliance achieves 14.5% cell efficiency on perovskite module," <https://www.pv-magazine.com/2018/04/09/solliance-achieves-14-5-cell-efficiency-on-perovskite-module/> (accessed: December 2018).
- [75] E. Tekin, P. J. Smith, U. S. Schubert, *Soft Matter* **2008**, *4*, 703.
- [76] B.-J. deGans, P. C. Duineveld, U. S. Schubert, *Adv. Mater.* **2004**, *16*, 203.
- [77] A. Teichler, J. Perelaer, U. S. Schubert, *J. Mater. Chem. C* **2013**, *1*, 1910.
- [78] J. Perelaer, P. J. Smith, D. Mager, D. Soltman, S. K. Volkman, V. Subramanian, J. G. Korvink, U. S. Schubert, *J. Mater. Chem.* **2010**, *20*, 8446.
- [79] Y. Sun, Y. Zhang, Q. Liang, Y. Zhang, H. Chi, Y. Shi, D. Fang, *RSC Adv.* **2013**, *3*, 11925.
- [80] Y.-S. Jung, K. Hwang, Y.-J. Heo, J.-E. Kim, D. Vak, D.-Y. Kim, *Adv. Opt. Mater.* **2018**, *6*, 1701182.
- [81] H. Peng, J. Yuan, S. Shen, M. Gao, A. S. R. Chesman, H. Yin, J. Cheng, Q. Zhang, D. Angmo, *Adv. Funct. Mater.* **2017**, *27*, 1703704.
- [82] J. E. Fromm, *IBM J. Res. Dev.* **1984**, *28*, 322.
- [83] N. Reis, B. Derby, *MRS Proc.* **2000**, *625*, 117.
- [84] B. J. De Gans, U. S. Schubert, *Langmuir* **2004**, *20*, 7789.
- [85] H. Hu, R. G. Larson, *J. Phys. Chem. B* **2006**, *110*, 7090.
- [86] C. N. Hoth, P. Schilinsky, S. A. Choulis, C. J. Brabec, *Nano Lett.* **2008**, *8*, 2806.
- [87] Z. Wei, H. Chen, K. Yan, S. Yang, *Angew. Chem., Int. Ed.* **2014**, *53*, 13239.
- [88] S.-G. Li, K.-J. Jiang, M.-J. Su, X.-P. Cui, J.-H. Huang, Q.-Q. Zhang, X.-Q. Zhou, L.-M. Yang, Y.-L. Song, *J. Mater. Chem. A* **2015**, *3*, 9092.
- [89] M. Bag, Z. Jiang, L. A. Renna, S. P. Jeong, V. M. Rotello, D. Venkataraman, *Mater. Lett.* **2016**, *164*, 472.
- [90] S. G. Hashmi, D. Martineau, X. Li, M. Ozkan, A. Tiihonen, M. I. Dar, T. Sarikka, S. M. Zakeeruddin, J. Paltakari, P. D. Lund, M. Grätzel, *Adv. Mater. Technol.* **2017**, *2*, 1600183.
- [91] F. Mathies, H. Eggers, B. S. Richards, G. Hernandez-Sosa, U. Lemmer, U. W. Paetzold, *ACS Appl. Energy Mater.* **2018**, *1*, 1834.
- [92] C. Liang, P. Li, H. Gu, Y. Zhang, F. Li, Y. Song, G. Shao, N. Mathews, G. Xing, *Sol. RRL* **2018**, *2*, 1770150.
- [93] P. Li, C. Liang, B. Bao, Y. Li, X. Hu, Y. Wang, Y. Zhang, F. Li, G. Shao, Y. Song, *Nano Energy* **2018**, *46*, 203.
- [94] S. Schliske, F. Mathies, D. Busko, N. Strobel, T. Rödlmeier, B. S. Richards, U. Lemmer, U. W. Paetzold, G. Hernandez-Sosa, E. Klampaftis, *ACS Appl. Energy Mater.* **2019**, *2*, 764.
- [95] T. Abzieher, S. Moghadamzadeh, F. Schackmar, H. Eggers, F. Sutterlütü, A. Farooq, D. Kojda, K. Habicht, R. Schmager, A. Mertens, R. Azmi, L. Kloth, J. A. Schwenzer, M. Hetterich, U. Lemmer, B. S. Richards, M. Powalla, U. W. Paetzold, *Adv. Energy Mater.* **2019**, *9*, 1802995.
- [96] A. Gheno, Y. Huang, J. Bouclé, B. Ratier, A. Rolland, J. Even, S. Vedraïne, *Sol. RRL* **2018**, *2*, 1800191.

- [97] J. E. Bishop, T. J. Routledge, D. G. Lidzey, *J. Phys. Chem. Lett.* **2018**, 9, 1977.
- [98] S. Razza, S. Castro-Hermosa, A. Di Carlo, T. M. Brown, *APL Mater.* **2016**, 4, 091508.
- [99] J. G. Tait, S. Manghooli, W. Qiu, L. Rakocevic, L. Kootstra, M. Jaysankar, C. A. Masse de la Huerta, U. W. Paetzold, R. Gehlhaar, D. Cheyens, P. Heremans, J. Poortmans, *J. Mater. Chem. A* **2016**, 4, 3792.
- [100] A. T. Barrows, A. J. Pearson, C. K. Kwak, A. D. F. Dunbar, A. R. Buckley, D. G. Lidzey, *Energy Environ. Sci.* **2014**, 7, 2944.
- [101] M. Ramesh, K. M. Boopathi, T. Y. Huang, Y. C. Huang, C. S. Tsao, C. W. Chu, *ACS Appl. Mater. Interfaces* **2015**, 7, 2359.
- [102] S. Das, B. Yang, G. Gu, P. C. Joshi, I. N. Ivanov, C. M. Rouleau, T. Aytug, D. B. Geohegan, K. Xiao, *ACS Photonics* **2015**, 2, 680.
- [103] X. Xia, W. Wu, H. Li, B. Zheng, Y. Xue, J. Xu, D. Zhang, C. Gao, X. Liu, *RSC Adv.* **2016**, 6, 14792.
- [104] H. Huang, J. Shi, L. Zhu, D. Li, Y. Luo, Q. Meng, *Nano Energy* **2016**, 27, 352.
- [105] J. E. Bishop, J. A. Smith, C. Greenland, V. Kumar, N. Vaenas, O. S. Game, T. J. Routledge, M. Wong-Stringer, C. Rodenburg, D. G. Lidzey, *ACS Appl. Mater. Interfaces* **2018**, 10, 39428.
- [106] S. Uličná, B. Dou, D. H. Kim, K. Zhu, J. M. Walls, J. W. Bowers, M. F. A. M. van Hest, *ACS Appl. Energy Mater.* **2018**, 1, 1853.
- [107] J. Troughton, D. Bryant, K. Wojciechowski, M. J. Carnie, H. Snaith, D. A. Worsley, T. M. Watson, *J. Mater. Chem. A* **2015**, 3, 9141.
- [108] I. S. Yang, M. R. Sohn, S. Do Sung, Y. J. Kim, Y. J. Yoo, J. Kim, W. I. Lee, *Nano Energy* **2017**, 32, 414.
- [109] J. E. Bishop, D. K. Mohamad, M. Wong-Stringer, A. Smith, D. G. Lidzey, *Sci. Rep.* **2017**, 7, 7962.
- [110] D. K. Mohamad, J. Griffin, C. Bracher, A. T. Barrows, D. G. Lidzey, *Adv. Energy Mater.* **2016**, 6, 1600994.
- [111] R. D. Deegan, O. Bakajin, T. F. Dupont, G. Huber, S. R. Nagel, T. a. Witten, *Phys. Rev. E: Stat. Phys., Plasmas, Fluids, Relat. Interdiscip. Top.* **2000**, 62, 756.
- [112] X. Fanton, A. M. Cazabat, *Langmuir* **1998**, 14, 2554.
- [113] Z. Ku, Y. Rong, M. Xu, T. Liu, H. Han, *Sci. Rep.* **2013**, 3, 3132.
- [114] Y. Yang, J. Xiao, H. Wei, L. Zhu, D. Li, Y. Luo, H. Wu, Q. Meng, *RSC Adv.* **2014**, 4, 52825.
- [115] F. Matteocci, S. Razza, F. Di Giacomo, S. Casaluci, G. Mincuzzi, T. M. Brown, A. D'Epifanio, S. Licocchia, A. Di Carlo, *Phys. Chem. Chem. Phys.* **2014**, 16, 3918.
- [116] L. Zhang, T. Liu, L. Liu, M. Hu, Y. Yang, A. Mei, H. Han, *J. Mater. Chem. A* **2015**, 3, 9165.
- [117] K. Cao, Z. Zuo, J. Cui, Y. Shen, T. Moehl, S. M. Zakeeruddin, M. Grätzel, M. Wang, *Nano Energy* **2015**, 17, 171.
- [118] Y. Hu, Z. Zhang, A. Mei, Y. Jiang, X. Hou, Q. Wang, K. Du, Y. Rong, Y. Zhou, G. Xu, H. Han, *Adv. Mater.* **2018**, 30, 1.
- [119] A. Kojima, K. Teshima, Y. Shirai, T. Miyasaka, *J. Am. Chem. Soc.* **2009**, 131, 6050.
- [120] Z. Ku, X. Xia, H. Shen, N. H. Tiep, H. J. Fan, *Nanoscale* **2015**, 7, 13363.
- [121] A. Mei, X. Li, L. Liu, Z. Ku, T. Liu, Y. Rong, M. Xu, M. Hu, J. Chen, Y. Yang, M. Grätzel, H. Han, *Science* **2014**, 345, 295.
- [122] C. Raminafshar, V. Dracopoulos, M. R. Mohammadi, P. Lianos, *Electrochim. Acta* **2018**, 276, 261.
- [123] Y. Hu, S. Si, A. Mei, Y. Rong, H. Liu, X. Li, H. Han, *Sol. RRL* **2017**, 1, 1600019.
- [124] G. Grancini, C. Roldán-Carmona, I. Zimmermann, E. Mosconi, X. Lee, D. Martineau, S. Narbey, F. Oswald, F. De Angelis, M. Graetzel, M. K. Nazeeruddin, *Nat. Commun.* **2017**, 8, 15684.
- [125] C. Kapnopoulos, E. D. Mekeridis, L. Tzounis, C. Polyzoidis, A. Zachariadis, S. Tsimikli, C. Gravalidis, A. Laskarakis, N. Vouroutzis, S. Logothetidis, *Sol. Energy Mater. Sol. Cells* **2016**, 144, 724.
- [126] M. Välimäki, P. Apilo, R. Po, E. Jansson, A. Bernardi, M. Ylikunnari, M. Vilkmann, G. Corso, J. Puustinen, J. Tuominen, J. Hast, *Nanoscale* **2015**, 7, 9570.
- [127] Q. Hu, H. Wu, J. Sun, D. Yan, Y. Gao, J. Yang, *Nanoscale* **2016**, 8, 5350.
- [128] H. J. Snaith, A. Abate, J. M. Ball, G. E. Eperon, T. Leijtens, N. K. Noel, S. D. Stranks, J. T. W. Wang, K. Wojciechowski, W. Zhang, *J. Phys. Chem. Lett.* **2014**, 5, 1511.
- [129] W. S. Yang, B.-W. Park, E. H. Jung, N. J. Jeon, Y. C. Kim, D. U. Lee, S. S. Shin, J. Seo, E. K. Kim, J. H. Noh, S. I. Seok, *Science* **2017**, 356, 1376.
- [130] N. J. Jeon, H. Na, E. H. Jung, T.-Y. Yang, Y. G. Lee, G. Kim, H.-W. Shin, S. Il Seok, J. Lee, J. Seo, *Nat. Energy* **2018**, 3, 682.
- [131] Y. Y. Kim, E. Y. Park, T.-Y. Yang, J. H. Noh, T. J. Shin, N. J. Jeon, J. Seo, *J. Mater. Chem. A* **2018**, 6, 12447.
- [132] F. Di Giacomo, S. Shanmugam, H. Fledderus, B. J. Bruijnaers, W. J. H. Verhees, M. S. Dorenkamper, S. C. Veenstra, W. Qiu, R. Gehlhaar, T. Merckx, T. Aernouts, R. Andriessen, Y. Galagan, *Sol. Energy Mater. Sol. Cells* **2018**, 181, 53.
- [133] M. A. Green, Y. Hishikawa, E. D. Dunlop, D. H. Levi, J. Hohl-Ebinger, A. W. Y. Ho-Baillie, *Prog. Photovoltaics Res. Appl.* **2018**, 26, 3.
- [134] Y. Deng, E. Peng, Y. Shao, Z. Xiao, Q. Dong, J. Huang, *Energy Environ. Sci.* **2015**, 8, 1544.
- [135] D. Vak, K. Hwang, A. Faulks, Y. S. Jung, N. Clark, D. Y. Kim, G. J. Wilson, S. E. Watkins, *Adv. Energy Mater.* **2015**, 5, 1401539.
- [136] L. Cai, L. Liang, J. Wu, B. Ding, L. Gao, B. Fan, *J. Semicond.* **2017**, 38, 014006.